Reactive collisions of sulfur dioxide with molten carbonates

Thomas Krebs and Gilbert M. Nathanson[1]

Department of Chemistry, University of Wisconsin–Madison, 1101 University Avenue, Madison, WI 53706-1322

Edited by Barbara J. Finlayson-Pitts, University of California, Irvine, CA, and approved December 28, 2009 (received for review October 4, 2009)

Molecular beam scattering experiments are used to investigate reactions of SO_2 at the surface of a molten alkali carbonate eutectic at 683 K. We find that two-thirds of the SO_2 molecules that thermalize at the surface of the melt are converted to gaseous CO_2 via the reaction $SO_2(g) + CO_3^{2-} \rightarrow CO_2(g) + SO_3^{2-}$. The CO_2 product is formed from SO_2 in less than 10^{-6} s, implying that the reaction takes place in a shallow liquid region less than 100 Å deep. The reaction probability does not vary between 683 and 883 K, further implying a compensation between decreasing SO_2 residence time in the near-interfacial region and increasing reactivity at higher temperatures. These results demonstrate the remarkable efficiency of $SO_2 \rightarrow CO_2$ conversion by molten carbonates, which appear to be much more reactive than dry calcium carbonate or wet slurries commonly used for flue gas desulfurization in coal-burning power plants.

flue gas desulfurization | gas scrubbing | gas–liquid reactions | liquid surface | molecular beam scattering

The atmospheric oxidation of sulfur dioxide produced during the combustion of fossil fuels is a significant source of acid rain and of fine aerosol particles harmful to human health (1–3). In coal-burning power plants, 75–98% of the SO_2 generated by combustion is removed by reaction with wet or dry limestone, which is predominantly composed of $CaCO_3$ (4). The overall reaction is (5):

$$SO_2(g) + CO_3^{2-} \rightarrow CO_2(g) + SO_3^{2-}. \qquad [1]$$

Numerous mechanistic (6–8) and kinetic (9, 10) studies of this reaction have been conducted by using solid $CaCO_3$ or limestone particles, with reported values of the activation energy ranging from 10 to 150 kJ mol^{-1} (9, 10). This large variation is probably caused by differences in the composition and porosity of the particles, the presence or absence of water vapor, and the buildup of a product overlayer (9). On the surface of dry $CaCO_3$, $SO_2 \rightarrow CO_2$ conversion takes place via the direct transfer of O^{2-} from CO_3^{2-} to a physisorbed SO_2 molecule (8). Adsorption of ambient water converts the solid surface into $Ca(OH)(CO_3H)$, which has been observed to enhance SO_2 uptake (6, 7). In the wet limestone process, SO_2 reacts with H_2O in the slurry to produce H^+ and HSO_3^-; these acidic species are neutralized by OH^- and HCO_3^- from dissolution of CO_3^{2-}, a process that generates CO_2 and leaves SO_3^{2-} in solution (5).

Oldenkamp and Margolin developed an alternative method to remove SO_2 from flue gases by employing a molten eutectic mixture of Li_2CO_3, Na_2CO_3, and K_2CO_3 (11). This liquid-phase reagent potentially avoids the wide variations in conditions observed for solid limestone and is regenerable (11, 12). When bubbling SO_2 through the carbonate melt at 800 K, nearly 100% of the SO_2 is removed for contact times as short as 0.05 s (12). In practice, this efficiency can be orders of magnitude higher than for solid $CaCO_3$ at the same reaction time. Measurements by van Houte and Delmon, for example, imply that only 10^{-5}% of the SO_2 is removed in 0.05 s, in part because the oxidation of product $CaSO_3$ produces a solid sulfate layer that impedes gas transport to the underlying solid carbonate (10).

The unusual reactivity of the carbonate melt and its low vapor pressure provide an opportunity to explore the conversion of SO_2 into CO_2 at the atomic scale by using gas–liquid scattering experiments, providing a direct comparison with SO_2 reactions on solid carbonates (6, 7). Fig. 1 illustrates the different pathways that an SO_2 molecule might encounter when impinging on the surface of molten carbonates. If the molecule has a translational energy much higher than the thermal energy of the liquid, it may inelastically scatter (IS) from the surface in one or a few collisions, retaining a significant fraction of its initial energy during the encounter (13). Alternatively, the incoming molecule may fully dissipate its excess kinetic energy through multiple collisions and become momentarily trapped at the surface of the melt. These trapped SO_2 molecules may then thermally desorb (TD) before or after diffusing into the melt or may react in the interfacial or bulk region with CO_3^{2-} to release CO_2. The scattering studies below provide a detailed picture of these events and show that SO_2 is readily converted into CO_2 within 10^{-6} s in a shallow region of the melt less than 100 Å thick.

Thermodynamic Properties of the Molten Carbonate Eutectic

The ternary alkali carbonate eutectic is composed of 44 mol% Li_2CO_3, 31 mol% Na_2CO_3, and 25 mol% K_2CO_3 and melts at 672 K (14). At this temperature, the viscosity of the mixture is 40 cP (15) and its surface tension is 240 dyn cm^{-1} (16). In the melt, the carbonate ion dissociates according to (17, 18)

$$CO_3^{2-} \rightleftharpoons CO_2(g) + O^{2-}, \qquad K_{diss} = P_{CO_2}[O^{2-}], \qquad [2]$$

where CO_2 and O^{2-} are the strongest acid and base that exist in solution, in analogy with H^+ and OH^- in water. This reaction has been studied by O^{2-} electrochemical titration at 973 K by Claes and coworkers (18). They determined that $K_{diss} = 10^{-5.4}$ M atm and $[O^{2-}]/P_{CO_2} = 0.1$ M atm^{-1}, which imply equilibrium values of $[O^{2-}] = 6 \times 10^{-4}$ M and $P_{CO_2} = 5$ Torr at 973 K. This vapor pressure is in excellent agreement with the predicted value of 4 Torr from extrapolation of CO_2 vapor pressure measurements between 1023 and 1223 K (19).

Intriguingly, Claes et al. postulated that CO_2 dissolved in the melt may react with CO_3^{2-} to generate the dicarbonate ion $C_2O_5^{2-}$ (18). This reactive solubility was estimated to be 50 times greater than the physical solubility of CO_2 at 973 K, such that $[C_2O_5^{2-}] = 50[CO_2]$. Eq. **2** imposes the constraint $[O^{2-}] = [CO_2] + [C_2O_5^{2-}]$, and therefore $[C_2O_5^{2-}] \approx [O^{2-}] = 6 \times 10^{-4}$ M and $[CO_2] = 1 \times 10^{-5}$ M at equilibrium. These numbers yield a Henry's law constant for physical solvation, $CO_2(g) \rightleftharpoons CO_2(soln)$, of $K_H(CO_2) = [CO_2]/P_{CO_2} = 0.002$ M atm^{-1} at 973 K. The dicarbonate reaction is relevant to our studies because

Author contributions: T.K. and G.M.N. designed research; T.K. performed research; T.K. and G.M.N. analyzed data; and T.K. and G.M.N. wrote the paper.

The authors declare no conflict of interest.

This article is a PNAS Direct Submission.

[1]To whom correspondence should be addressed. E-mail: nathanson@chem.wisc.edu.

This article contains supporting information online at www.pnas.org/cgi/content/full/0910993107/DCSupplemental.

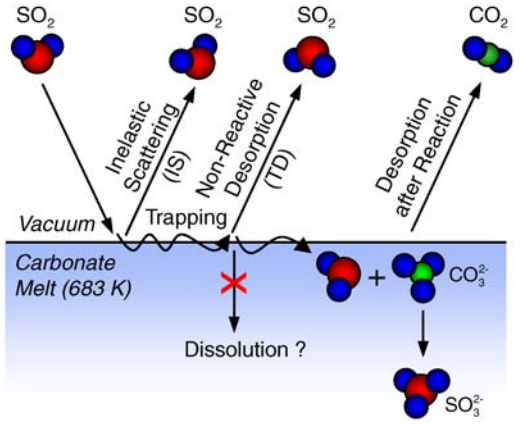

Fig. 1. Scattering and reaction pathways for an SO_2 molecule striking the surface of a molten carbonate.

CO_2 generated by reaction of SO_2 within the melt may in turn be transformed into $C_2O_5^{2-}$ before evaporating. As discussed below, our experiments imply that nearly all CO_2 molecules escape rather than form $C_2O_5^{2-}$.

Unfortunately, no values of K_{diss} or $K_H(CO_2)$ have been recorded at the eutectic point of 672 K. Our CO_2 evaporation measurements provide rough limits of $K_{diss} < 10^{-13}$ M atm and $K_H < 10^2$ M atm^{-1} (*SI Text*). An extrapolation of the vapor pressure measurements (19) to 672 K predicts an equilibrium CO_2 vapor pressure of 10^{-4} Torr. The O^{2-} concentration based on these values is less than 10^{-6} M. This value lies well below the measured maximum solubility of O^{2-} of 0.02 M (0.0004 mol fraction) in the melt at 672 K (20).

There is also no thermodynamic data for the reaction of SO_2 in molten carbonates. One comparison is to the conversion of solid Na_2CO_3 to solid Na_2SO_3 via $SO_2(g) + Na_2CO_3(s) \rightleftharpoons CO_2(g) + Na_2SO_3(s)$. At 672 K, this reaction is exothermic by 66 kJ mol^{-1} and reaches equilibrium at $P_{CO_2}/P_{SO_2} \approx 1,200$, in accord with the favorable reactivity of SO_2 in the eutectic.

Results

Gas–Liquid Scattering Experiments. Fig. 2 depicts the scattering geometry, which allows a monoenergetic beam of gas molecules to strike the molten carbonate at a 55° angle. Product molecules leaving the liquid at 55° are chopped into 70-μs pulses by a spinning postchopper wheel. They then travel a distance d_{post} between the wheel and mass spectrometer, where their arrival times t_{final} are recorded as TOF spectra. In this postchopper configuration, t_{final} can be converted into a velocity $v_{final} = d_{post}/t_{final}$ and translational energy $E_{final} = \frac{1}{2} m_{gas} v_{final}^2$ of the exiting molecule (13).

Alternatively, the incident gas beam can be chopped before the molecules reach the molten carbonate (13, 22). In this prechopper configuration, the beam is chopped into 70-μs pulses that strike the liquid in 1.2-ms intervals. The arrival time at the mass spectrometer is the sum of the gas-phase flight times of the molecule before and after interaction with the liquid *and* the residence time of the dissolved species in solution. As shown previously, this pulsed-beam technique can be used to measure average bulk-phase residence times from 10^{-6} to 10^{-2} s (13, 22).

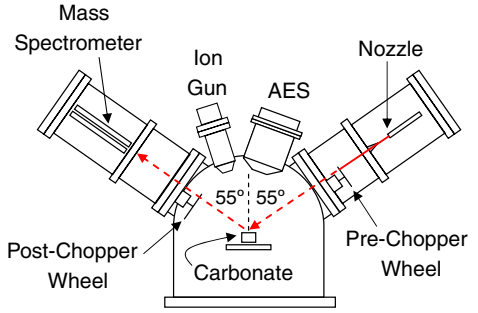

Fig. 2. Drawing of the experimental apparatus. "AES" denotes Auger electron spectrometer.

Auger Electron and Argon Scattering Measurements of Surface Purity. Before the start of each experiment, the alkali carbonate eutectic is melted in vacuum at 683 K and sputtered with 2 keV Ar^+ ions for 30 min to remove surface contaminants. Auger electron spectra recorded before and after sputtering are shown in Fig. 3*A* for the elements C, K, and O; the Li and Na transition probabilities lead to small signals (23) and are not shown. The C/O ratio, which would provide the best measure of surface cleanliness, could not be determined because of overlap of the C and K transitions. Fig. 3*A* does show, however, that the carbon signal drops by ~30% upon sputtering, implying that sputtering leads to a reduction in carbon-containing impurities at the melt surface. We also searched for evidence of SO_3^{2-} from reaction of SO_2 and CO_3^{2-} that might accumulate at the surface of the melt, but no sulfur signal was observed even after three weeks of experiments.

Previous studies in our laboratory have shown that high-energy argon atom scattering can also be used to gauge the presence of surface impurities because of the changes in surface mass and surface roughness that occur upon segregation of the impurity species (24). Fig. 3*B* shows postchopper TOF spectra of 90 kJ mol^{-1} Ar atoms scattering from the surface of the carbonate melt before and after the sample was sputtered. The spectra consist predominantly of a sharp peak at early arrival times that is assigned to Ar atoms that IS after one or a few bounces along the surface and a weaker signal at longer arrival times that is assigned to Ar atoms that dissipate their energy and TD. Fig. 3*B* reveals that the peak intensity grows upon sputtering and that the average energy loss in the IS channel drops from 71% to 65%. This reduction in energy transfer and gain in intensity reflect an increase in the effective surface mass and decrease in surface roughness because of

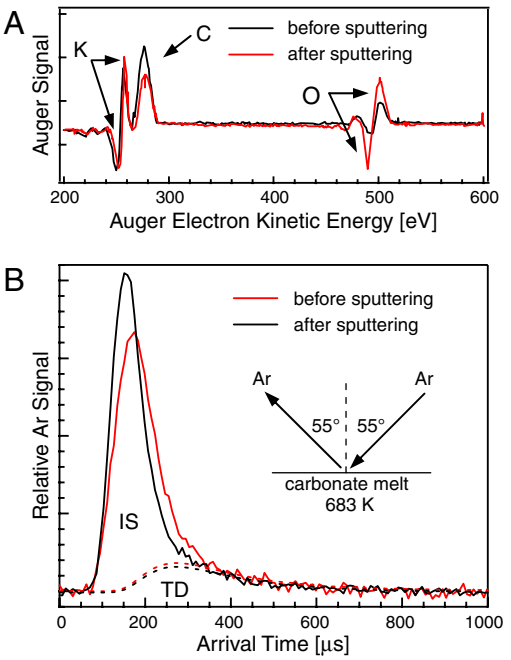

Fig. 3. (*A*) Auger electron spectra of the molten alkali carbonate at 683 K before and after sputtering. (*B*) Postchopper TOF spectra of 90 kJ mol^{-1} Ar atoms scattering from the carbonate mixture at 683 K before and after s puttering. "IS" and "TD" denote inelastic scattering and thermal desorption, respectively. The dashed TD lines represent a MB distribution at 683 K.

removal of impurities, such as hydrocarbons, during the sputtering process (13, 24). All Ar spectra recorded after sputtering were highly reproducible, indicating that the impurities did not reappear over the course of the experiment.

Scattering and Uptake of SO_2 in Collisions with Molten Carbonate. The reaction of SO_2 with CO_3^{2-} was monitored at SO_2 collision energies of 16 and 240 kJ mol^{-1} and liquid temperatures of 683–883 K in order to investigate thermalization and reaction of SO_2 with the melt under different conditions. Both postchopper and prechopper spectra were recorded to measure the relative fluxes of the scattered SO_2 reagent and the CO_2 reaction product and the combined residence times of these species in the carbonate solution.

Thermal Energy SO_2 Scattering. We first report collisions of SO_2 molecules with an incident energy $E_{inc} = 16$ kJ mol^{-1}, which is only 50% greater than the average thermal energy of a gas at $T_{liq} = 683$ K, given by $2RT_{liq} = 11$ kJ mol^{-1}. Fig. 4*A* displays postchopper (green) and prechopper (red) TOF spectra of scattered SO_2 molecules that did not react upon collision. Both spectra are plotted on the postchopper time axis by correcting the prechopper arrival times for the longer flight path from the prechopper wheel, as depicted in Fig. 2 (22). They are also normalized at the peaks to account for differences in transmission of molecules through the post- and prechopper wheels. The two spectra have identical shapes, and each are well fit by a Maxwell–Boltzmann (MB) distribution at $T_{liq} = 683$ K (black). The good MB fit implies that these low-energy SO_2 molecules dissipate their excess translational energy and thermally equilibrate upon collision before desorbing back into the gas phase.

The overlap between the post- and prechopper spectra further implies that the residence time of unreacted SO_2 molecules in the carbonate mixture is less than 10^{-6} s, the shortest time that we can infer from overlapping spectra (22). When the average solvation time exceeds 10^{-6} s, a fraction of the solute molecules diffuse deeply into the liquid and desorb over a range of times that measurably broaden and shift the MB desorption distribution to later arrival times in the prechopper spectrum. A residence time τ characteristic of this desorption may be obtained by invoking flux balance at the gas–liquid boundary and solving the diffusion equation. In this continuum model, τ is the time in which the outgoing gas flux reaches 57% of the incoming flux as the liquid becomes saturated with gas (13, 22):

$$\tau = D\left(\frac{4K_H RT_{liq}}{\alpha\langle v\rangle}\right)^2. \qquad [3]$$

D and K_H are the diffusion constant and physical solubility of SO_2 in the melt, respectively, α is the SO_2 entry probability under thermal collision conditions, and $\langle v\rangle = (8k_B T/\pi m_{SO_2})^{1/2}$. The desorption profiles generated by the diffusion equation are convoluted with an MB distribution to produce the $\tau = 1$ (blue) and 10 μs (gray) desorption spectra in Fig. 4*A*. The $\tau = 0$ μs curve (black) is equal to the MB distribution itself. The $\tau = 1$ and 10 μs curves are broader than the measured TOF spectra and confirm that the characteristic desorption time is less than 10^{-6} s. This upper limit corresponds to the time for an SO_2 molecule to traverse in and out of the melt, during which it may diffuse an average distance of $(D\tau/2)^{1/2} < 100$ Å before desorbing for $D = 10^{-6}$ cm^2 s^{-1}, estimated from the melt viscosity of ~40 cP at 683 K. This depth corresponds to ~20 monolayers of the carbonate mixture.

Eq. **3** can be used to predict an upper limit to the physical solubility of SO_2 in the melt by assuming submicrosecond solvation. For $\tau < 10^{-6}$ s, $T_{liq} = 683$ K, and $\alpha \approx 1$, the maximum SO_2 solubility $K_H(SO_2)$ is 10^2 M atm^{-1}. The actual SO_2 solubility is likely to be much smaller; the closest comparison we could find is the solubility of SO_2 in 88 wt% sulfuric acid (16 M H_2SO_4) at 393 K, which is ~0.1 M atm^{-1} (25). A similarly low solubility for SO_2 in the eutectic would predict a bulk-phase residence time of 10^{-12} s

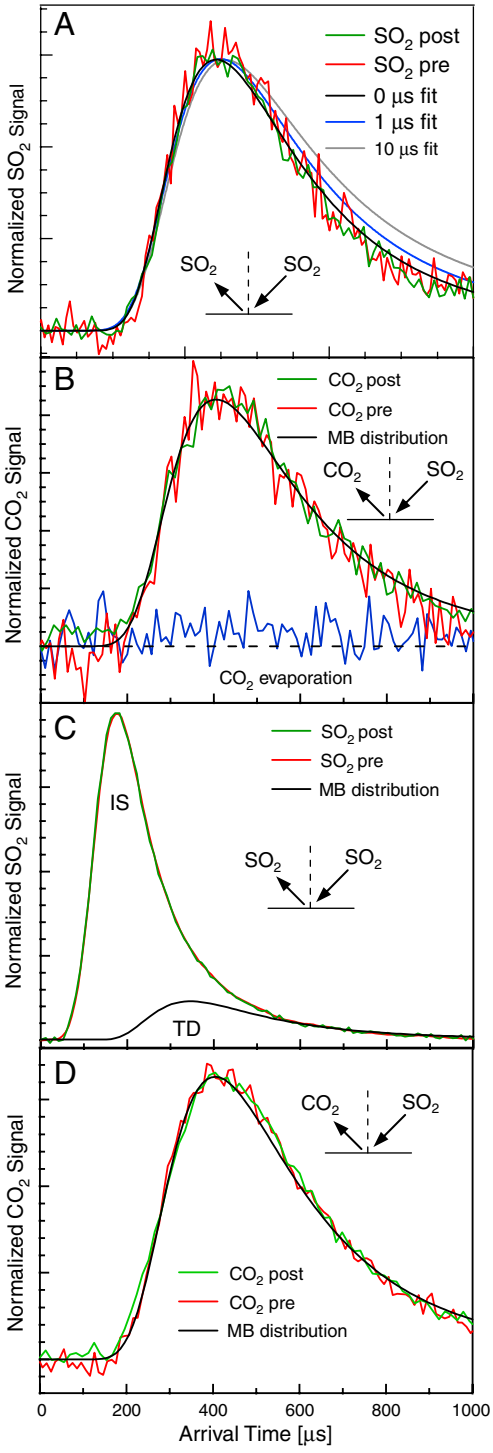

Fig. 4. (*A*) Postchopper (green) and prechopper (red) TOF spectra of 16 kJ mol^{-1} SO_2 molecules scattering from the carbonate melt at 683 K. The calculated TOF spectra correspond to $\tau = 0$ μs(blue), $\tau = 1$ μs (blue), and $\tau = 10$ μs (gray) bulk-phase residence times. (*B*) Post- and prechopper spectra for CO_2 desorption after $SO_2 \rightarrow CO_2$ conversion following collisions of 16 kJ mol^{-1} SO_2. The weak postchopper spectrum (blue) corresponds to CO_2 evaporation in the absence of SO_2. (*C*) Post- and prechopper spectra of 240 kJ mol^{-1} SO_2 molecules scattering from the carbonate melt. The two spectra are identical. (*D*) Post- and prechopper spectra of CO_2 desorption following collisions of 240 kJ mol^{-1} SO_2.

and a diffusion depth of 0.1 Å. These small values lie outside the applicability of Eq. **3** and instead imply that most SO_2 molecules react or desorb before penetrating beyond the interfacial region.

Fig. 4*B*, our most important finding, demonstrates that CO_2 molecules desorb from the melt upon exposure to SO_2 at $E_{inc} = 16\ kJ\ mol^{-1}$ and $T_{liq} = 683$ K. The CO_2 post- and prechopper spectra have identical shapes, and each are well fit by an MB distribution at T_{liq}. This good fit signifies that the product CO_2 molecules are thermally equilibrated before they desorb from the melt, and the good overlap between the post- and prechopper spectra indicates that the combined CO_2 and SO_2 bulk-phase reaction and residence times must be less than 10^{-6} s. As calculated above, this short time implies that the physical solubility of CO_2, like SO_2, is less than $10^2\ M\ atm^{-1}$. The submicrosecond solvation time further demonstrates that the conversion of SO_2 into CO_2 must occur within a depth of 100 Å. In the limit that τ is much less than 10^{-6} s, $CO_2 \rightarrow SO_2$ conversion would occur within an even shallower region close to the outermost layer. We note that all CO_2 and SO_2 TOF spectra were unchanged over the several-hour period of each experiment, implying that the surface of the molten carbonate remained fresh and did not become covered with a solid sulfite film.

SO_2 Reaction Probabilities. The actual fraction of molecules that react upon collision with the melt can be measured in two ways: by monitoring the appearance of CO_2 and by monitoring the disappearance of SO_2. The first method relies on a comparison of the fluxes of thermally desorbing reagent SO_2 and product CO_2 molecules. We assume that the thermally desorbing species in Fig. 4*A* and *B* have the same angular distributions, which are likely cosine in shape (13, 26). Thus, the ratio of the SO_2 and CO_2 desorption fluxes $I^{TD}_{SO_2}$ and $I^{TD}_{CO_2}$ at the observation angle of 55° obtained from the TOF spectra is equal to the ratio of fluxes integrated over all exit angles. The mass spectrometer signals must be adjusted for the different ionization probabilities and mass spectrometer sensitivities at $m/z = 64$ (SO_2) and 44 (CO_2) and for their isotopic abundances, as calculated in *SI Text*. The $SO_2 \rightarrow CO_2$ reaction probability p_{react} is then computed from the flux of SO_2 molecules that did not react and the flux of SO_2 molecules that are converted to CO_2, assuming no SO_2 remains in the melt:

$$p_{react} = \frac{I^{TD}_{CO_2}}{I^{TD}_{SO_2} + I^{TD}_{CO_2}}. \quad [4]$$

This probability is found to be 0.68 ± 0.04 (95% confidence interval) at $E_{inc} = 16\ kJ\ mol^{-1}$ from 12 individual measurements of the SO_2 and CO_2 TOF spectra. Thus, at a collision energy close to $2RT_{liq}$, where nearly all molecules thermalize upon collision, two of every three impinging SO_2 molecules are converted into CO_2 in the near-interfacial region.

The SO_2 reaction probability may also be obtained by using the King and Wells uptake method to monitor the disappearance of SO_2 rather than the appearance of CO_2. In this second method, the uptake probability is given by (13)

$$p_{uptake} = \frac{P_{flag} - P_{open}}{P_{flag} - P_{back}}, \quad [5]$$

where P_{flag} and P_{open} denote the partial pressures of the reactant SO_2 gas when the beam is blocked by a Teflon flag and when it strikes the liquid, respectively, and P_{back} denotes the partial background pressure of the reactant gas. Each partial pressure was measured with the mass spectrometer in 600-s intervals. The uptake probability differs from the $SO_2 \rightarrow CO_2$ reaction probability p_{react} because it includes all processes that lead to disappearance of SO_2. In addition to conversion of SO_2 to CO_2, these processes include the direct reaction of SO_2 with dissolved O^{2-} to generate SO_3^{2-} and the conversion of product CO_2 to $C_2O_5^{2-}$. We find that $p_{uptake} = 0.60 \pm 0.02$ for SO_2 at $E_{inc} = 16\ kJ\ mol^{-1}$ (12 measurements), which is smaller than $p_{react} = 0.68 \pm 0.04$ using the same carbonate sample. The 0.08 difference in p_{uptake} and p_{react} likely arises from variations in measurement technique, as described in *SI Text*. Because p_{uptake} is not larger than p_{react}, there appears to be no other reaction channel that competes with $SO_2 \rightarrow CO_2$ conversion, thereby excluding significant production of $C_2O_5^{2-}$ from CO_2 or reaction of SO_2 with trace O^{2-} during the submicrosecond SO_2 solvation time in the melt.

Hyperthermal SO_2 Scattering. Comparisons at low and high SO_2 collision energies provide additional insight into the reaction mechanism. Fig. 4*C* displays post- and prechopper TOF spectra of unreacted SO_2 following collisions of SO_2 at $240\ kJ\ mol^{-1}$ ($42RT_{liq}$). The most prominent new feature is a sharp peak at early arrival times, which is composed of SO_2 molecules recoiling directly from the surface, as depicted in Fig. 1. These inelastically scattered molecules escape reaction but still lose most of their energy, departing with an average kinetic energy of only $40\ kJ\ mol^{-1}$. The spectra also exhibit a longtime tail, which is fit to an MB distribution and assigned to SO_2 molecules that dissipate their excess energy and TD from the surface before reacting.

The overlapping CO_2 post- and prechopper spectra in Fig. 4*D* show that, as in the case of low-energy SO_2, the CO_2 product molecules are created from SO_2 in less than 10^{-6} s. These product molecules then desorb in a thermal distribution. The absence of nonthermal CO_2 desorption indicates that the CO_2 molecules are not ejected from the surface upon sputtering by the high-energy SO_2 molecules. At least two mechanisms may lead to thermal desorption of CO_2: The impinging SO_2 molecules may react directly with CO_3^{2-} to produce CO_2 molecules that thermally equilibrate before desorbing, or the SO_2 molecules may first thermalize and then react with CO_3^{2-} in the near-interfacial region, generating CO_2 molecules that thermally equilibrate and desorb. To choose between them, we calculate p_{react} for collisions at $240\ kJ\ mol^{-1}$ by using only the SO_2 thermal desorption component in Fig. 4*C*. The value of p_{react} is 0.68 ± 0.05 (9 measurements), equal to the 0.68 ± 0.04 value for $16\ kJ\ mol^{-1}$ collisions. This equality implies that the SO_2 molecules first fully dissipate their excess energy through collisions with surface alkali and carbonate ions, losing memory of their initial trajectories, and then react with CO_3^{2-} near the surface to form CO_2 (26). This two-step trapping and reaction pathway is also found in other gas–liquid systems, including the dissociation of gaseous HCl in sulfuric acid (13).

Temperature Dependence of SO_2 Reactivity. The SO_2 reaction probability might be expected to vary with liquid temperature because of a barrier to reaction or changes in the SO_2 residence time at the surface or in the melt. To address this question, five reaction probabilities were measured in 50 K intervals from 683 to 883 K for collisions of $16\ kJ\ mol^{-1}$ SO_2. At each temperature, the SO_2 and CO_2 pre- and postchopper spectra were fit well by an MB distribution at T_{liq}. The spectra were measured in the sequence $683 \rightarrow 733 \rightarrow 783$ K and $683 \rightarrow 833 \rightarrow 883$ K, and then the sequences were repeated. Each experiment started at 683 K to test whether CO_2 evaporation at higher temperatures altered the melt. The four p_{react} values at 683 K were within 0.03 of each other, indicating that CO_2 evaporation did not significantly increase the O^{2-} concentration. Fig. 5 displays the measured probabilities. Remarkably, they show no measurable change in $SO_2 \rightarrow CO_2$ conversion rates over the 200-K range. The average value of p_{react} is 0.74 ± 0.01 for all 12 measurements. This average is slightly higher than $p_{react} = 0.68 \pm 0.04$ at 683 K reported above; the data were recorded by using different samples, which

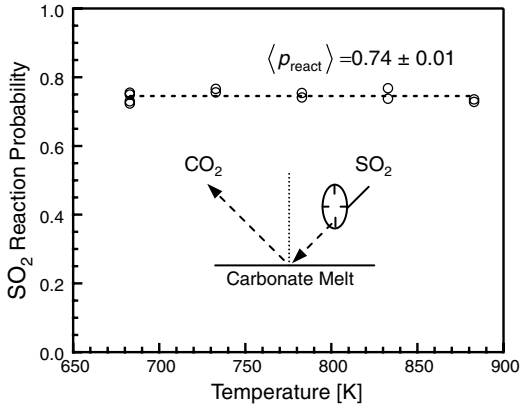

Fig. 5. SO_2 reaction probability versus temperature of the carbonate melt. The values of p_{react} are calculated from Eq **4**.

might account for the difference. McIlroy et al. also did not observe changes in SO_2 uptake into the eutectic mixture from the melting point to 920 K, but they attributed this insensitivity to gas-phase diffusion limitations in their high-pressure reactor (12). The data in Fig. 5 show that the gas–liquid reaction itself does not vary with temperature.

Discussion

The scattering experiments demonstrate that SO_2 readily reacts in the near-interfacial region of the molten alkali carbonate eutectic, proceeding more quickly than at the surface of dry limestone or in aqueous limestone suspensions. Our measured steady-state reaction and uptake probabilities span 0.60–0.74. In comparison, the uptake of SO_2 on calcium carbonate powders has been measured to be 0.01–0.1 on partially hydrated surfaces composed of $CaCO_3$ and $Ca(OH)(HCO_3)$ (7, 27). When referenced to the internal surface area of the powders, these uptake probabilities may drop to values as low as 10^{-4} (8). Additionally, droplet train experiments show that the uptake of SO_2 into water at pH < 10 is only ~0.04, suggesting that the entry of SO_2 into limestone slurries does not exceed this value (28).

The large reaction probability for the molten carbonate must arise in part from the high density and mobility of the CO_3^{2-} and alkali ions, allowing them to surround thermalized SO_2 molecules in the interfacial region. We do not have direct information about the composition of the molten surface layer or orientations of the CO_3^{2-} ions. However, the surface tensions of ternary carbonate solutions are well predicted by ideal solution relations (16). This agreement implies little segregation of the Li^+, K^+, or Na^+ ions, as expected for a hot mixture; the top layers of the melt should then be composed of both CO_3^{2-} and cations in order to preserve electrical neutrality. In this case, the heavy incoming SO_2 molecule will undergo repeated collisions with both CO_3^{2-} and alkali ions, each time dissipating more energy until it is trapped in the gas-surface potential created by the continually moving ions.

The measured submicrosecond time for $SO_2 \rightarrow CO_2$ conversion implies that the transfer of O^{2-} from CO_3^{2-} to SO_2 occurs within a near-surface region less than 20 layers deep. This transfer may be analogous to simulations of SO_2 reactions with solid CaO and MgO (29, 30). Within this picture, O^{2-} jumps from CO_3^{2-} to the strong Lewis acid SO_2 when the S atom points toward one of the negatively charged O atoms of CO_3^{2-} and each O atom of SO_2 points toward a K^+, Na^+, or Li^+ ion. This transfer creates solvated SO_3^{2-} ions while releasing CO_2, a weaker Lewis acid. Our measurements indicate that a pathway such as this one fails in only one of every three encounters, most likely because the adsorbed SO_2 molecule is propelled back into vacuum by thermal motions of the surface species before reaching a reactive configuration.

Fig. 5 shows further that the $SO_2 \rightarrow CO_2$ reaction probability remains constant over the temperature range from 683 to 883 K. This result is remarkable because the SO_2 adsorption and solvation time should drop with increasing temperature, implying that the $SO_2 \rightarrow CO_2$ reaction rate rises to just balance the reduced SO_2 contact time. Alternatively, incoming SO_2 molecules may react directly with surface CO_3^{2-} ions in a nearly barrierless O^{2-} transfer that bypasses the SO_2 thermal accommodation step, a pathway that is likely to be less sensitive to temperature (26). However, the measurements of p_{react} described above argue against direct reaction in favor of a two-step SO_2 trapping and reaction pathway. We hope that additional measurements using molten alkali hydroxides (31) and different alkali carbonate mixtures will provide deeper insight into the balance between SO_2 residence time and reactivity as well as the possibility of a direct $SO_2 \rightarrow CO_2$ gas-surface reaction.

From a practical viewpoint, the insensitivity to temperature may be advantageous because it implies that efficient SO_2 removal is not confined to temperatures near the eutectic point, where product SO_3^{2-} ions (or SO_4^{2-} ions upon oxidation) may be less soluble or cause solidification of the melt upon extended exposure (12). This insensitivity, when combined with the near-interfacial conversion of $SO_2 \rightarrow CO_2$, suggests that thin flowing films or coatings of molten carbonates over a wide temperature range may efficiently remove SO_2 from waste gases.

Materials/Methods

The Li_2CO_3, Na_2CO_3, and K_2CO_3 powders (Sigma-Aldrich, 99 + %) were mixed and dried at 423 K for 2 h. When the mixture was heated in vacuum (base pressure = 2×10^{-9} Torr) to 683 K for the first time, a gray film appeared on the surface of the otherwise transparent melt. This film was scraped away with a silver wire in vacuum and did not reappear. The carbonate sample is contained in a 2-mm-deep by 19-mm-diameter crucible machined from silver because of its excellent corrosion resistance (21). No silver signal could be detected in the Auger spectra, indicating that the carbonate melt does not react with the crucible.

Beams of Ar and SO_2 are created by supersonic expansion of each gas through a 0.08-mm-diameter nozzle, heated to 383 K to suppress formation of clusters. A high translational energy beam of 240 kJ mol^{-1} SO_2 was obtained by using 2 mol% SO_2 seeded in H_2. A 16 kJ mol^{-1} beam of 2 mol% SO_2 was formed by bubbling Ar through a 0.5 mass% aqueous solution of SO_2 at 273 K, where the SO_2 vapor pressure is 11 Torr.

ACKNOWLEDGMENTS. This material is based upon work supported by the National Science Foundation under Grant CHE-0809681. We are grateful to the National Science Foundation for funding this work and to the Deutsche Forschungsgemeinschaft for a research fellowship (to T.K.) under Grant KR 2935/2-1.

1. Finlayson-Pitts BJ, Pitts JN (2000) *Chemistry of the Upper and Lower Atmosphere* (Academic, New York).
2. Bricker OP, Rice KC (1993) Acid rain. *Annu Rev Earth Pl Sc* 21:151–174.
3. U.S. Environmental Protection Agency Sulfur dioxide. www.epa.gov/oar/urbanair/so2/.
4. Srivastava RK, Jozewicz W (2001) Flue gas desulfurization: The state of the art. *J Air Waste Manage* 51:1676–1688.
5. U.S. Environmental Protection Agency Flue gas desulfurization (acid removal). yosemite.epa.gov/oaqps/EOGtrain.nsf/DisplayView/SI_412C_9?OpenDocument.
6. Al-Hosney HA, Grassian VH (2005) Water, sulfur dioxide, and nitric acid adsorption on calcium carbonate: A transmission and ATR-FTIR study. *Phys Chem Chem Phys* 7:1266–1276.
7. Santschi C, Rossi MJ (2006) Uptake of CO_2, SO_2, HNO_3 and HCl on calcite ($CaCO_3$) at 300 K: Mechanism and the role of adsorbed water. *J Phys Chem A* 110:6789–6802.
8. Thompson MM, Palmer RA (1988) *In situ* Fourier transform infrared diffuse reflectance and photoacoustic spectroscopy characterization of sulfur-oxygen species resulting from the reaction of SO_2 with $CaCO_3$. *Appl Spectrosc* 42:945–951.
9. Hu G, Dam-Johansen K, Wedel S, Hansen JP (2006) Review of the direct sulfation reaction of limestone. *Prog Energ Combust* 32:386–407.
10. van Houte G, Delmon B (1978) Kinetics of reaction of $CaCO_3$ with SO_2 and O_2 below 650 °C. *Bull Soc Chim Belg* 87:241–249.
11. Oldenkamp RD, Margolin ED (1969) The molten carbonate process for sulfur oxide emissions. *Chem Eng Prog* 65:73–76.

12. McIlroy RA, Atwood GA, Major CJ (1973) Absorption of sulfur dioxide by molten carbonates. *Environ Sci Technol* 7:1022–1028.
13. Nathanson GM (2004) Molecular beam studies of gas-liquid interfaces. *Annu Rev Phys Chem* 55:231–255.
14. Janz GJ, Lorenz MR (1961) Solid-liquid phase equilibria for mixtures of lithium, sodium, and potassium carbonates. *J Chem Eng Data* 6:321–323.
15. Ejima T, et al. (1987) Viscosity of the eutectic Li_2CO_3-Na_2CO_3-K_2CO_3 melt. *J Chem Eng Data* 32:180–182.
16. Kojima T, Miyazaki Y, Nomura K, Tanimoto K (2008) Density, surface tension, and electrical conductivity of ternary molten carbonate system Li_2CO_3-Na_2CO_3-K_2CO_3 and methods for their estimation. *J Electrochem Soc* 155:F150–F156.
17. Janz GJ (1967) Molten carbonate electrolytes as acid-base solvent systems. *J Chem Educ* 44:581–590.
18. Claes P, Moyaux D, Peeters D (1999) Solubility and solvation of carbon dioxide in the molten $Li_2CO_3/Na_2CO_3/K_2CO_3$ (43.5:31.5:25.0 mol-%) eutectic mixture at 973 K. I. Experimental part. *Eur J Inorg Chem* 4:583–588.
19. Spedding PL, Mills R (1965) Trace-ion diffusion (and vapor pressure) in molten alkali carbonates. *J Electrochem Soc* 112:594–599.
20. White SH, Twardoch UM (1989) The solubility and electrochemistry of alkali metal oxides in the molten eutectic mixture of lithium carbonate-sodium carbonate-potassium carbonate. *J Appl Electrochem* 19:901–910.
21. Wyatt M, Fisher JM (1988) Control of corrosion in molten carbonate fuel cells—The application of platinum group metals in anode components. *Platinum Met Rev* 32:200–203.
22. Morris JR, et al. (2000) Molecular beam scattering from supercooled sulfuric acid: Collisions of HCl, HBr, and HNO_3 with 70 wt% D_2SO_4. *J Phys Chem A* 104:6738–6751.
23. Davis LE (1976) *Handbook of Auger Electron Spectra* (Physical Electronics, Eden Prairie, MN).
24. Lawrence JR, Glass SV, Nathanson GM (2005) Evaporation of water through butanol films at the surface of supercooled sulfuric acid. *J Phys Chem A* 109:7449–7457.
25. Zhang Q, Wang H, Dalla Lana IG, Chuang KT (1998) Solubility of sulfur dioxide in sulfuric acid of high concentration. *Ind Eng Chem Res* 37:1167–1172.
26. Rettner CT, Auerbach DH (1994) Distinguishing the direct and indirect products of a gas-surface reaction. *Science* 263:365–367.
27. Usher CR, Al-Hosney H, Carlos-Cullar S, Grassian VH (2002) A laboratory study of the heterogeneous uptake and oxidation of sulfur dioxide on mineral dust particles. *J Geophys Res-Atmos* 107:4713.
28. Boniface J, et al. (2000) Uptake of SO_2, H_2S and CO_2 by aqueous solutions. *J Phys Chem A* 104:7502–7510.
29. Pacchioni G, Ricart JM, Illas F (1994) Ab initio cluster model calculations on the chemisorption of CO_2 and SO_2 probe molecules on MgO and CaO (100) surfaces. A theoretical measure of basicity. *J Am Chem Soc* 116:10152–10158.
30. Rodriguez JA, Jirsak T, Freitag A, Larese JZ, Maiti A (2000) Interaction of SO_2 with MgO (100) and Cu/MgO (100): Decomposition reactions and the formation of SO_3 and SO_4. *J Phys Chem B* 104:7439–7448.
31. Ho C-S, Shih S-M, Liu C-F, Chu H-M, Lee C-D (2002) Kinetics of the sulfation of $Ca(OH)_2$ at low temperatures. *Ind Eng Chem Res* 41:3357–3364.